Available online at www.sciencedirect.com
ScienceDirect
Journal of Sound and Vibration 323 (2009) 896–909
JOURNAL OF SOUND AND VIBRATION
www.elsevier.com/locate/jsvi

An iterated maps approach for dynamic ratchetting in sdof hysteretic damping systems

I.-S. Ahn*, S.S. Chen, G.F. Dargush

Department of Civil, Structural and Environmental Engineering, University at Buffalo, State University of New York, Buffalo, NY 14260, USA

Received 20 March 2007; received in revised form 4 January 2009; accepted 8 January 2009
Handling Editor: C.L. Morfey
Available online 20 February 2009

Abstract

Dynamic ratchetting is a phenomenon in which plastic deformation increases in successive cycles. In the present paper, first, various characteristics of dynamic ratchetting are demonstrated based on numerical simulation. Second, iterated maps are developed as a tool for the investigation of dynamic ratchetting in a single degree of freedom (sdof) system. When an elasto-perfectly-plastic model is employed to represent hysteretic damping, a piecewise linear solution can be obtained and used to develop iterated maps. A stability investigation in the iterated maps shows that dynamic ratchetting is developed under a stable cycling. In this stable cycling, dynamic ratchetting occurs when an excitation function loses antiperiodicity (shift symmetry).

1. Introduction

Hysteresis is a material characteristic that exhibits different loading and unloading paths in the stress–strain relationship for given stress or strain ranges [1]. Through hysteretic motion, energy in the system is dissipated and, for example, this hysteretic damping is one of the major energy dissipation mechanisms used in the seismic design of civil structures [2,3].

When multi-frequency sinusoidal excitations are applied to hysteretic damping systems, it is shown that the plastic displacement may continuously increase in successive cycles [4]. This phenomenon is identified and referred to as dynamic ratchetting in Ref. [5]. The occurrence of dynamic ratchetting depends on the plasticity model used and excitation frequencies. Specifically, an elasto-perfectly-plastic model shows significant dynamic ratchetting when excitation frequencies are commensurable and the product of terms comprising the ratio is an even number. Dynamic ratchetting is a kind of ratchet, which in Ref. [6] is defined as "realization of systems which produce a direct current (transport) from a fluctuating environment in the absence of gradient and net forces." Among ratchet phenomena in various systems and on various occasions [7], dynamic ratchetting has an unique aspect that restoring forces are piecewise continuous functions, instead of

*Corresponding author.
E-mail addresses: iahn@buffalo.edu (I.-S. Ahn), ciechen@eng.buffalo.edu (S.S. Chen), gdargush@eng.buffalo.edu (G.F. Dargush).

0022-460X/$ - see front matter © 2009 Elsevier Ltd. All rights reserved.
doi:10.1016/j.jsv.2009.01.009

continuous functions derived from a potential function. Dynamic ratchetting has similarity to the more ordinary ratchetting behavior found in material plasticity. In material plasticity, when applied stress cycles have a nonzero mean, ratchetting may occur, resulting in a shortfall of safety and serviceability due to excessive plastic deformation or due to excessive cycles of low-cycle fatigue [1,8]. The same consequences may be expected through dynamic ratchetting under sinusoidal excitations and earthquakes [4].

In the present paper, iterated maps are introduced to investigate the evolution and stability of dynamic ratchetting in hysteretic damping systems with an elasto-perfectly-plastic model. Iterated maps can be developed from numerical methods, but here the piecewise linear solutions are employed instead. Piecewise linear solutions are not analytical solutions that provide an explicit relationship between input and output or between parameters and output. However, when feasible, piecewise solutions provide significant in-depth information for dynamic systems. The development of piecewise linear solution can be found in various dynamic systems such as vibro-impact systems [9,10], bi-linear systems [11,12], friction systems [13], and slider systems with an impacting mass [14–16].

In various nonlinear dynamic systems, an iterated maps approach is a powerful tool for the investigation of motion. The adoption of iterated maps for vibro-impact system and hysteretic damping system can be found in Refs. [9,17], respectively. The similarities and differences between the present study and [17] are discussed in following sections. Due to inherited limitations of iterated maps, it is difficult or impractical to apply this approach to dynamic systems having more than one variable. The simplicity and efficiency of iterated maps cannot be maintained in multi degrees-of-freedom systems or systems with more complicated plasticity models. Consequently, here the focus is on single degree of freedom (sdof) elasto-perfectly-plastic systems.

2. Governing equations and piecewise linear solution

When a mass, m, connected to an elasto-perfectly-plastic hysteretic damping element, is subjected to multi-frequency excitations as in Fig. 1(a), the dynamic governing equation becomes:

$$m\frac{\mathrm{d}^2U}{\mathrm{d}t'^2}+F\left(U,\frac{\mathrm{d}U}{\mathrm{d}t'}\right)=\sum_{i=1}^{M}P_i\sin\Omega_i't', \tag{1}$$

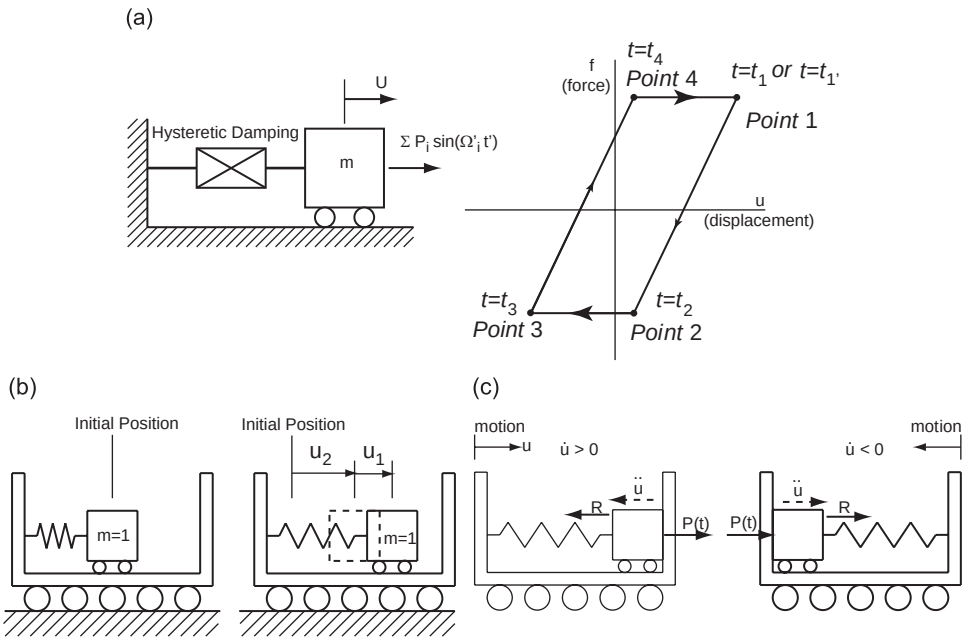

Fig. 1. Single degree of freedom hysteretic damping model: (a) Force-displacement relationship, (b) Cart model for elasto-perfectly-plastic model, and (c) Free body diagrams.

with

$$\frac{F}{\mathrm{d}t'}\left(U,\frac{\mathrm{d}U}{\mathrm{d}t'}\right)=\begin{cases}k\dfrac{\mathrm{d}U}{\mathrm{d}t'} & \text{if } F^2<F_y^2,\\ 0 & \text{else,}\end{cases}$$

where t' is real time, M represents number of excitation frequencies, k is pre-yielding stiffness, and F_y is yielding force.

The definition of force-rate, $\mathrm{d}F/\mathrm{d}t'$, is derived by integrating the stress rate–strain rate material plasticity relationship over the domain. The effects from viscous damping will also be investigated in a later section. After the introduction of yielding displacement $U_y=F_y/k$, the nondimensional version of Eq. (1) is expressed as

$$\ddot{u}+f(u,\dot{u})=E(t), \tag{2}$$

with

$$E(t)=\sum_{i=1}^{M}p_i\,\sin\Omega_i t\,;\quad \dot{f}(u,\dot{u})=\begin{cases}\dot{u} & \text{if } f^2<1,\\ 0 & \text{else,}\end{cases}$$

where $T'=\sqrt{m/k}=1/\omega$, $t=t'/T'$, $u=U/U_y$, $p_i=T'^2/mU_yP_i$, $\Omega_i=\Omega_i'T'=\Omega_i'/\omega$, and $\dot{u}=\mathrm{d}u/\mathrm{d}t$. Notice that in Eq. (2), $\dot{u}$ is used for the derivative with respect to nondimensional time t.

In Fig. 1(b), the dynamic motion of a sdof hysteretic damping system is presented by a mass loaded in a massless cart connected by springs to the wall. When excitations are applied to the mass, the mass will oscillate. If the amplitude of oscillation increases, the mass touches the wall, and both will move together. Two displacements are introduced; u_1 represents the distance from the center of the cart to the center of the mass, and u_2 represents the distance of the center of the cart from the initial position. When accounting for the motion with hysteretic damping, the yield surface of the elasto-perfectly-plastic model corresponds to the wall of the cart. The cart can move freely to the left or right, which simulates the movement of the yield surface in the elasto-perfectly-plastic model. Following this analogy, the elastic and plastic deformations of the body are equivalent to u_1 and u_2, respectively. Thus,

$$u=u_e+u_p,\quad u_e=u_1,\quad u_p=u_2, \tag{3}$$

where u_e is the elastic deformation and u_p is the plastic deformation.

Based on the mass in the cart model in Fig. 1(b), the governing equations of dynamic motion are developed. Until the mass touches the wall, the motion of the mass is linear forced vibration such as:

$$\ddot{u}_e+u_e=\sum_{i=1}^{M}p_i\,\sin\Omega_i t. \tag{4}$$

If the mass touches the wall (when $|u_e|=1$), the cart will move with the mass, ignoring any bounce of the mass. Free-body diagrams in Fig. 1(c) show two possible scenarios. The force R in the diagram is the spring force when it is deformed by 1 (i.e., by a unit nondimensional yield displacement). The governing equation for each case becomes:

$$\begin{aligned}\ddot{u}_p+R&=\sum_{i=1}^{M}p_i\sin\Omega_i t\quad \text{for } \dot{u}_p>0,\\ \ddot{u}_p-R&=\sum_{i=1}^{M}p_i\sin\Omega_i t\quad \text{for } \dot{u}_p<0.\end{aligned} \tag{5}$$

The solution of Eq. (4) can be written

$$\begin{Bmatrix}u_e\\ \dot{u}_e\end{Bmatrix}=\begin{pmatrix}\sin(t) & \cos(t)\\ \cos(t) & -\sin(t)\end{pmatrix}\begin{Bmatrix}A\\ B\end{Bmatrix}+\begin{Bmatrix}\sum_{i=1}^{M}\dfrac{p_i}{(1-\Omega_i^2)}\sin\Omega_i t\\ \sum_{i=1}^{M}\dfrac{\Omega_i p_i}{(1-\Omega_i^2)}\cos\Omega_i t\end{Bmatrix}, \tag{6}$$

while the solution of Eq. (5) becomes:

$$\begin{Bmatrix} u_p \\ \dot{u}_p \end{Bmatrix} = \begin{pmatrix} t & 1 \\ 1 & 0 \end{pmatrix} \begin{Bmatrix} C \\ D \end{Bmatrix} + \begin{Bmatrix} \pm\frac{R}{2}t^2 - \sum_{i=1}^{M} \frac{p_i}{\Omega_i^2} \sin \Omega_i t \\ \pm Rt - \sum_{i=1}^{M} \frac{\Omega_i p_i}{\Omega_i} \cos \Omega_i t \end{Bmatrix}. \tag{7}$$

The + sign in the terms $(R/2)t^2$ and Rt in Eq. (7) corresponds to the case when $\dot{u}_p < 0$ (and − sign for $\dot{u}_p > 0$). Constants, A, B, C, and D are determined from known displacement, u_o, and velocity, $\dot{u}_o$, at a specific time t_o.

The change of state from elastic to plastic occurs when the mass hits the cart as in Fig. 1(c), which corresponds to the moment when an elastic deformation, u_e, is either 1 or −1. The change from plastic to elastic occurs when the velocity changes its sign. At the points of state change in Fig. 1(a), elastic deformation (u_{eo}), plastic deformation (u_{po}), and velocity ($\dot{u}$) at each point, 1, 2, 3, 4, and (1′) can be pre-defined as

$$\begin{aligned}
&\text{Point 1: } t = t_1, u_{eo} = 1, u_{po} = u_p, \dot{u} = 0,\\
&\text{Point 2: } t = t_2, u_{eo} = -1, u_{po} = u_p, \dot{u} = \dot{u}_e(t_2),\\
&\text{Point 3: } t = t_3, u_{eo} = -1, u_{po} = u_p + \Delta u_p^-, \dot{u} = 0,\\
&\text{Point 4: } t = t_4, u_{eo} = 1, u_{po} = u_p + \Delta u_p^-, \dot{u} = \dot{u}_e(t_4),\\
&\text{Point 1}' : \ t = t_{1'}, u_{eo} = 1, u_{po} = u_p + \Delta u_p^- + \Delta u_p^+, \dot{u} = 0.
\end{aligned}$$

If the current motion is in an elastic state (between *Point 1* and *Point 2* or between *Point 3* and *Point 4* in Fig. 1(a)), the transition time t_2 from elastic to the lower branch of plastic response and the transition time t_4 from elastic to the upper branch of plastic response are determined by solving Eq. (8), such as

$$\begin{aligned}
u_e(t_2) &= A \sin(t_2) + B \cos(t_2) + \sum_{i=1}^{M} \frac{p_i}{(1-\Omega_i^2)} \sin \Omega_i t_2 = -1,\\
u_e(t_4) &= A \sin(t_4) + B \cos(t_4) + \sum_{i=1}^{M} \frac{p_i}{(1-\Omega_i^2)} \sin \Omega_i t_4 = 1.
\end{aligned} \tag{8}$$

Also the transition times, t_3 and $t_{1'}$, from plastic to elastic response are determined by solving the following equations:

$$\begin{aligned}
\dot{u}_p(t_3) &= C + Rt_3 - \sum_{i=1}^{M} \frac{p_i}{\Omega_i} \cos \Omega_i t_3 = 0,\\
\dot{u}_p(t_{1'}) &= C - Rt_{1'} - \sum_{i=1}^{M} \frac{p_i}{\Omega_i} \cos \Omega_i t_{1'} = 0.
\end{aligned} \tag{9}$$

Because the solutions of each state (elastic or plastic) and the conditions of transition are known, the dynamic motion can be determined uniquely for a given initial condition. However, a closed-form solution cannot be obtained because there are no analytical solutions for Eqs. (8) and (9). To acquire transition times, a numerical solver such as the Newton–Raphson technique can be utilized. In a later section, piecewise linear solutions are used for the development of iterated maps.

3. Dynamic ratchetting behavior

Dynamic ratchetting is a phenomenon such that the plastic deformation increases continuously in successive cycles in hysteretic damping dynamic systems. In particular, this phenomenon can only be observed when the frequencies of an excitation are in integer ratios, i.e. commensurable, and the product of terms comprising the ratio is an even number. In order to characterize dynamic ratchetting, the governing equation, Eq. (2), is solved by the Runge–Kutta method. In the analyses, the time step is 0.01 seconds or $\frac{1}{20}$th of the smallest period between excitation frequencies. In Fig. 2, responses from three different viscous damping values are compared

where ξ is the nondimensional critical damping ratio. Although the level of ξ influences the amount of accumulated deformation, dynamic ratchetting does occur even in the presence of significant viscous damping. In the following discussion, therefore, viscous damping is not included.

Fig. 3 shows a contour plot of absolute values of the maximum displacements for 2,000 nondimensional time units. Amplitudes of applied excitations are fixed to 1.0, i.e. $p_1 = p_2 = 1$, and frequencies are changed from 0.0 to 5.0. The corresponding three-dimensional plot is added in the upper right side. Out-of-range regions near the origin are not from dynamic ratchetting, but from the nearly static loading situation. The regions having dynamic ratchetting are arranged by lines corresponding to specific frequency ratios. Dynamic ratchetting becomes significant when two applied frequencies are represented by an integer ratio, $n : m$, and their product $n \times m$, is an even number. So $n : m = 1 : 2, 2 : 3, 2 : 5, \ldots$ are cases that have severe dynamic

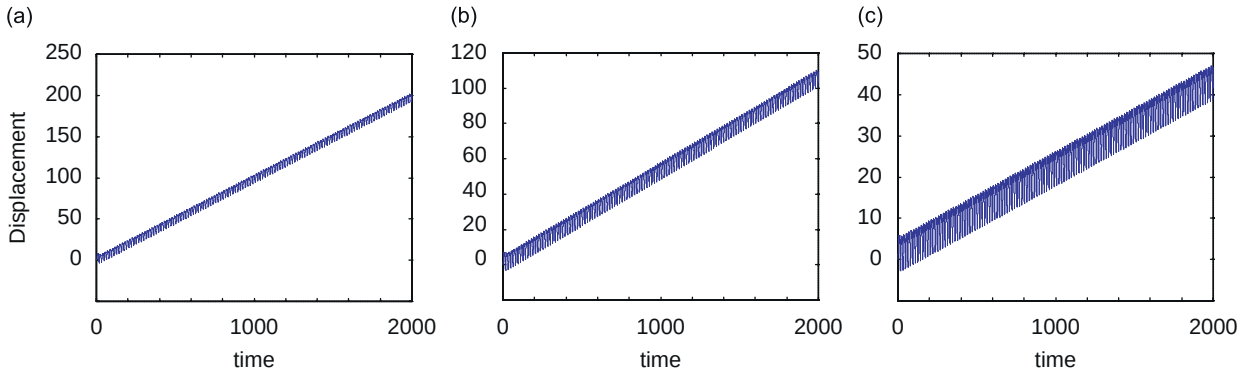

Fig. 2. Sensitivity of dynamic ratchetting to viscous damping ($\Omega_1 = 0.8, \Omega_2 = 0.4$): (a) $\xi = 0.03$, (b) $\xi = 0.05$, and (c) $\xi = 0.1$.

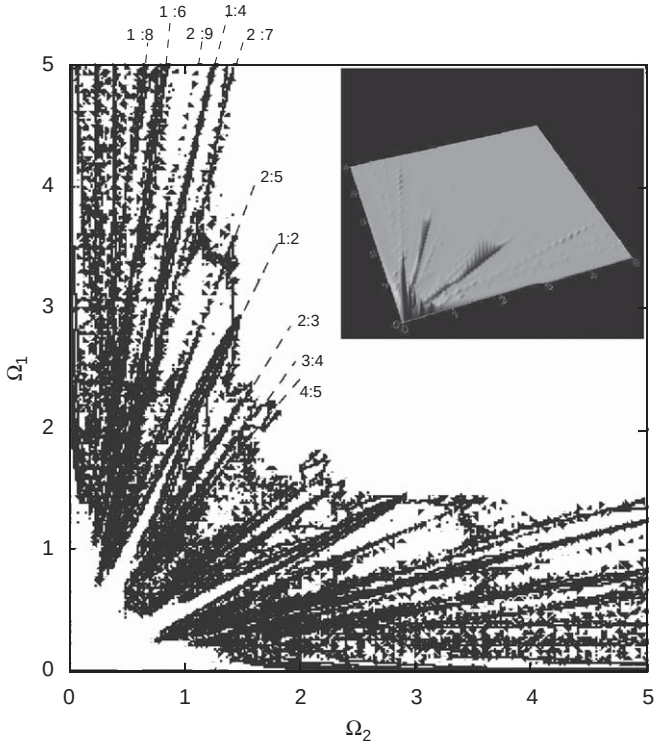

Fig. 3. Contour plot of absolute maximum displacement ($p_1 = p_2 = 1.0$).

ratchetting, but there is no dynamic ratchetting when $n:m=1:3,1:5,3:5,\ldots$. Another observation is dynamic ratchetting effects are greater if the $n\times m$ value is smaller. For example, compare 1:2 and 1:8 cases.

In Fig. 4, four Poincaré sections [18] of 1:4 commensurable frequencies are generated for four different amplitudes of excitations. For this, and all subsequent Poincaré section plots, $2\pi/\Omega_1$ is used for the sampling period. Based on this sampling rate, displacement, velocity, and the restoring force are taken and used to generate the Poincaré section. When the amplitudes are small in Figs. 4(a) and (b), the observed limit-cyclic motions are represented by four discrete points. When the amplitude increases, the four points translate in the force–displacement plane with bounded velocities as in Figs. 4(c) and (d). This translation of the displacement in the force-displacement plane corresponds to dynamic ratchetting.

Fig. 5 depicts the Poincaré sections of incommensurable frequencies. With $\Omega_1=0.8$ and $\Omega_2\approx\sqrt{2}/5$, the frequency ratio is close to 1:4, which can be compared to Fig. 4. For incommensurable frequencies, figures show quasi-periodic motions, which are bounded even for larger amplitudes of excitations. More specifically, four ellipses from mostly linear oscillations are observed when amplitudes are small. These ellipses coalesce into one closed curve (Figs. 5(b) and (c)) when amplitudes increase.

These changes are presented for another frequency combination in Fig. 6, where $\Omega_1=4.0$ and $\Omega_2\approx\sqrt{2}$ are used. When the amplitude is small (Fig. 6(a)), the contribution from the natural frequency (i.e. 1.0) is shown as four distinct sets of points because of the 1:4 frequency ratio. The contribution from the frequency $\sqrt{2}$ can be identified by a circular shape because of quasi-periodic motions from the $1:\sqrt{2}$ frequency ratio. When the amplitude increases, the size of ellipses increases, and ellipses are overlapped (Figs. 6(b) and (c)). Under larger amplitude, four ellipses from the $1:\sqrt{2}$ combination coalesce into one ellipse because of the $\sqrt{2}:4$ combination (Figs. 6(d) and (e)). In Fig. 6(f), the large ellipse from the $\sqrt{2}:4$ combination survives for even larger amplitude and makes the motion bounded.

When three frequencies are employed in the excitation functions, the same argument can be made. Dynamic ratchetting does not occur if the product of the integer ratios, $m\times n\times k$, makes an odd number. Fig. 7 shows displacement time histories of two such cases. To make this argument applicable to M frequency excitations, it

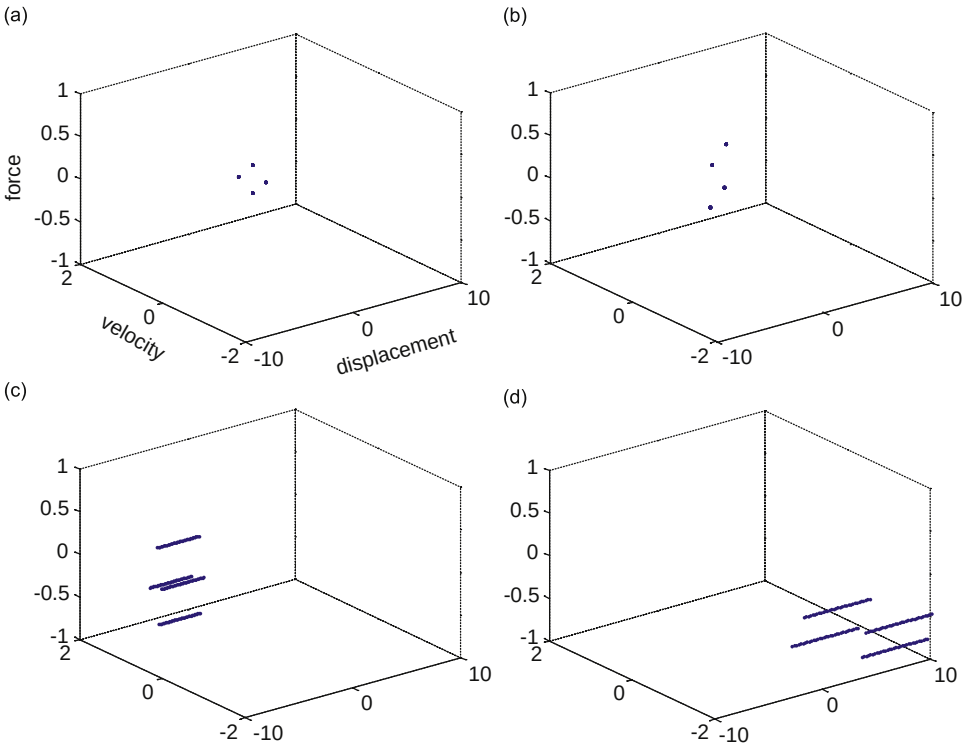

Fig. 4. Poincaré sections for commensurable frequency excitations ($\Omega_1=0.8,\Omega_2=0.2$): (a) $p_1=p_2=0.2$, (b) $p_1=p_2=0.25$, (c) $p_1=p_2=0.3$, and (d) $p_1=p_2=0.5$.

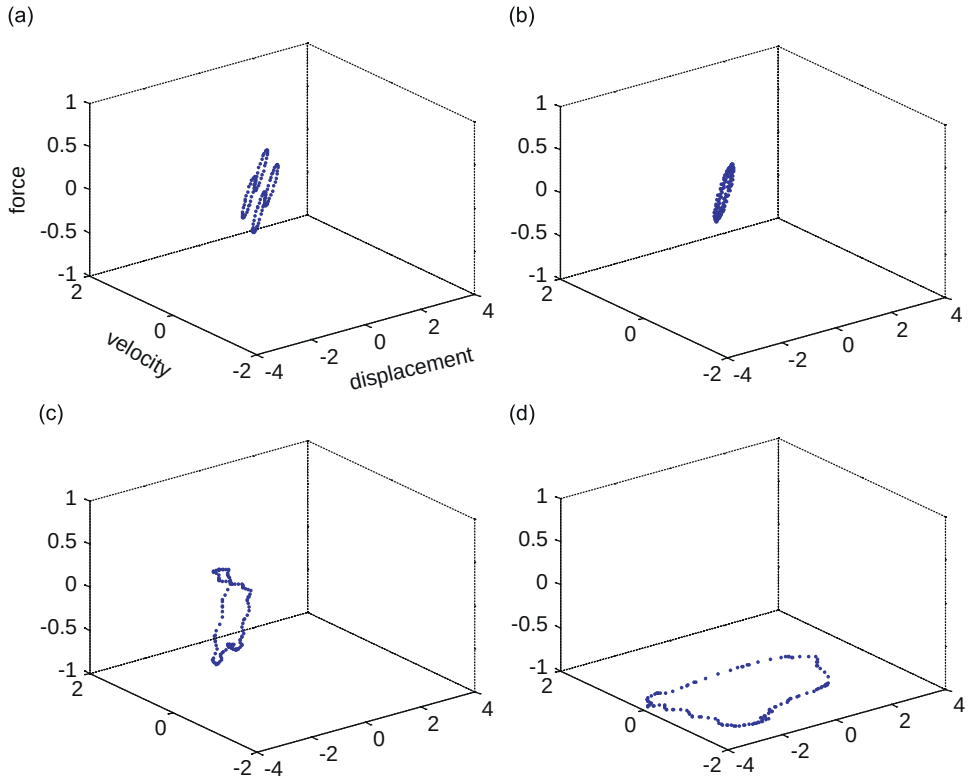

Fig. 5. Poincaré sections for incommensurable frequency excitations ($\Omega_1 = 0.8, \Omega_2 \approx \sqrt{2}/5$): (a) $p_1 = p_2 = 0.2$, (b) $p_1 = p_2 = 0.25$, (c) $p_1 = p_2 = 0.3$, and (d) $p_1 = p_2 = 0.5$.

can be stated that there is no dynamic ratchetting in commensurable frequency excitations if the product of integers in the frequency ratio is an odd number such as:

$$\prod_{i=1}^{M} r_i = \text{ odd number}, \tag{10}$$

where

$$\frac{\Omega_1}{r_1} = \frac{\Omega_2}{r_2} = \cdots = \frac{\Omega_m}{r_m}.$$

This condition is satisfied only if all r_i are odd numbers, which is a very rare case in M commensurable frequency excitations. Therefore, most multi-frequency excitations contain more than one frequency combination that can develop dynamic ratchetting.

4. Iterated maps

Many of the techniques used in contemporary research on nonlinear dynamical systems originate from the work of Poincaré [18]. In particular, iterated maps have been used for the investigation of various nonlinear dynamic problems [19–22]. For some piecewise linear dynamic systems, the number of variables is reduced to one so that an iterated maps approach becomes a powerful tool. Shaw and Holmes [9] used iterated maps for a perfectly plastic vibro-impact system, where discontinuous map functions were used for stability investigation. Miller and Butler [17] developed iterated maps for an elasto-perfectly-plastic hysteretic damping system. In these studies, transition time, when the motion changes from one state to another, was taken as an

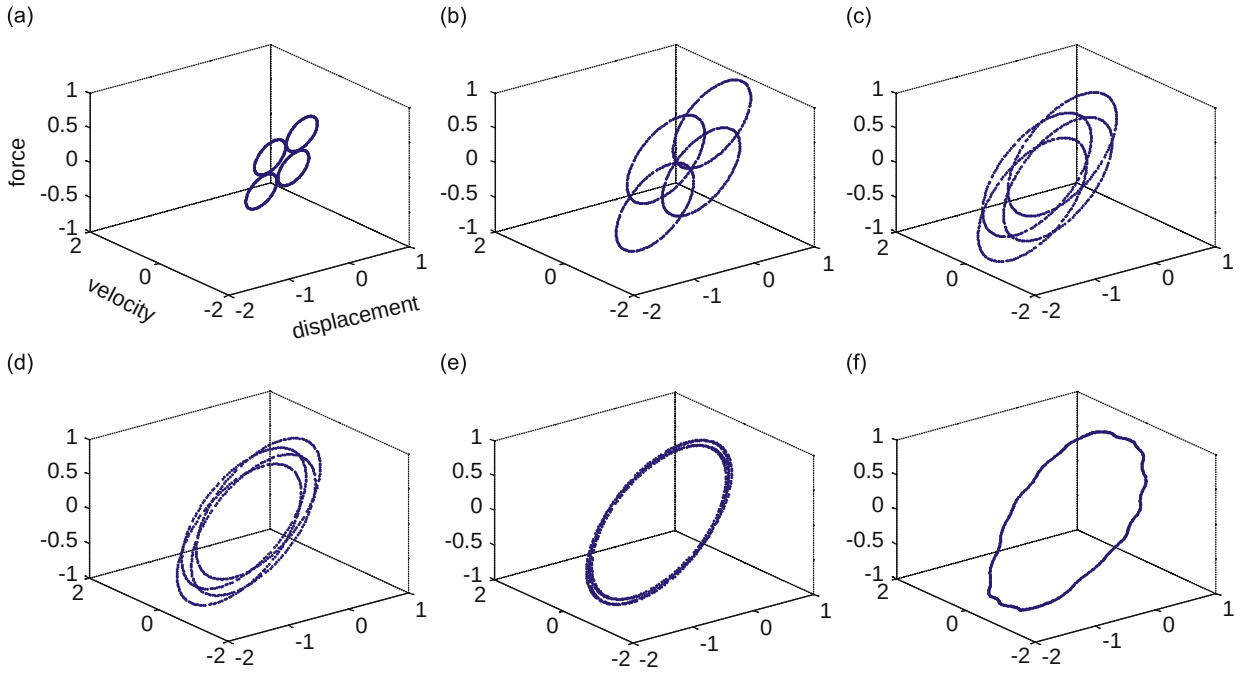

Fig. 6. Poincaré sections for incommensurable frequency excitations ($\Omega_1 = 4, \Omega_2 \approx \sqrt{2}$): (a) $p_1 = p_2 = 0.2$, (b) $p_1 = p_2 = 0.5$, (c) $p_1 = p_2 = 0.7$, (d) $p_1 = p_2 = 0.8$, (e) $p_1 = p_2 = 0.9$, and (f) $p_1 = p_2 = 1.0$.

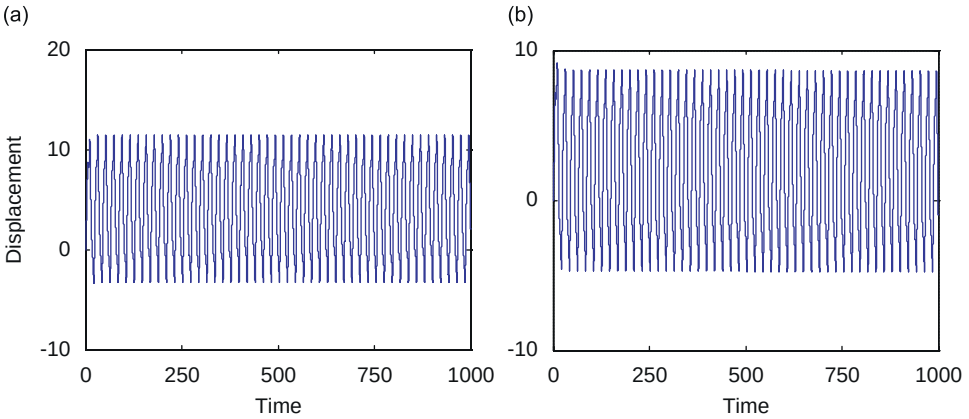

Fig. 7. Responses of three commensurable frequencies: (a) $\Omega_1 = 0.3$, $\Omega_2 = 0.9$, $\Omega_3 = 1.5$, and (b) $\Omega_1 = 0.3$, $\Omega_2 = 0.9$, $\Omega_3 = 2.1$.

independent variable. Applying iterated maps in Ref. [17] to dynamic ratchetting, however, has a limitation because only single frequency excitations were considered.

A stable hysteretic loop should include at least one of each *Point 1* (state **p**) and *Point 3* (state **m**) in Fig. 1(a). The maps from one state to another are obtained from the relations given in Eqs. (6) and (7). For example, when the current state is **p** at time t_1, the known elastic displacement ($u_e = 1$) and velocity ($\dot{u} = 0$) are used to calculate constants A and B in Eq. (6). The times t_2 and t_4 are known by solving Eq. (8). Two constants C and D are also determined from the plastic displacement and velocity at this moment. For the known t_2, the upper equation in Eq. (9) is used to acquire t_3, and the lower one is used to acquire t_1' from the known t_4. When this procedure is repeated for varying t_1, the relationship from t_1 to t_3 and from t_1 to t_1' can be obtained, which consists of the **p–m** map and **p–p** map, respectively. Between two possible states, **m** will follow if $t_2 < t_4$.

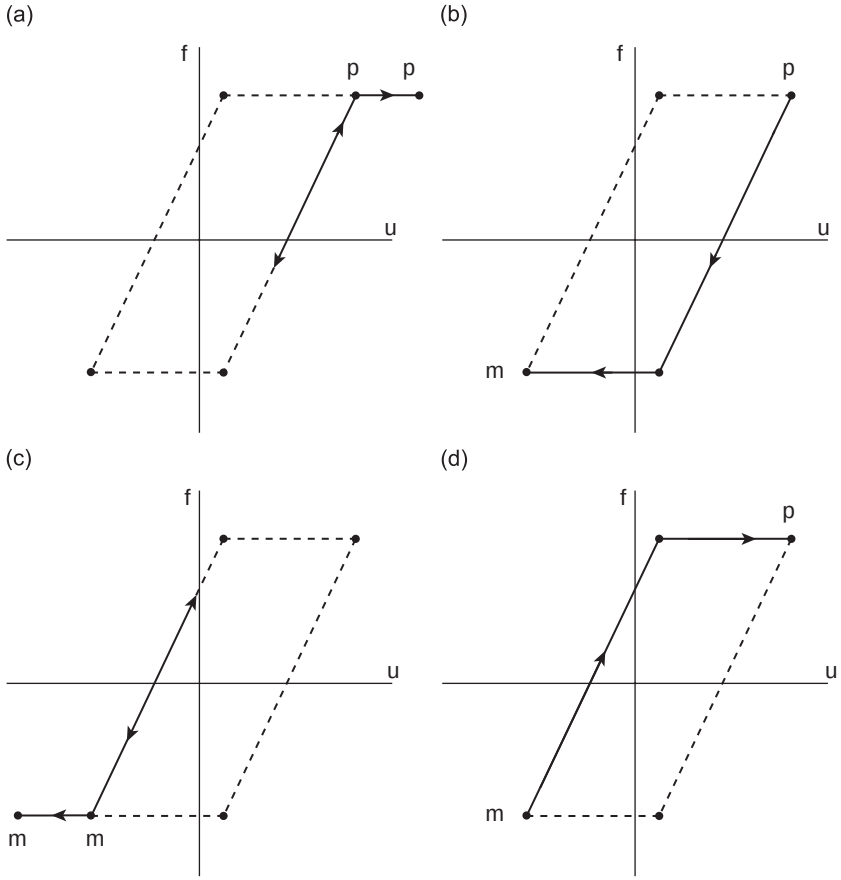

Fig. 8. Behavior of iterated maps: (a) **p–p** map, (b) **p–m** map, (c) **m–m** map, and (d) **m–p** map.

Otherwise **p** will follow. In the investigation of dynamic ratchetting, four maps, **p–m**, **p–p**, **m–p**, and **m–m** maps, are necessary to represent dynamic motion. The maps derived in Ref. [17] were **p–m** and **m–p** maps, and the shape of the two are the same.

When τ_i is used to represent the modulus of time t_i in Fig. 1(a) to the fixed period of motion T, such as

$$\tau_i = \text{ the remainder of } \left(\frac{t_i}{T}\right), \quad 0 \leqslant \tau_i < 1, \quad i = 1,2,3,4, \tag{11}$$

the definition of four maps thus becomes

$$\begin{aligned} &\mathbf{p}-\mathbf{p} \text{ map: } \tau_1 = f_p^p(\tau_1),\\ &\mathbf{p}-\mathbf{m} \text{ map: } \tau_3 = f_p^m(\tau_1),\\ &\mathbf{m}-\mathbf{p} \text{ map: } \tau_1 = f_m^p(\tau_3),\\ &\mathbf{m}-\mathbf{m} \text{ map: } \tau_3 = f_m^m(\tau_3). \end{aligned} \tag{12}$$

Fig. 8 shows the behavior of each map function schematically.

In iterated maps, the $\tau(n)$ axis represents τ_1 or τ_3 in the current state and the $\tau(n+1)$ axis represents τ_1 or τ_3 in the following state. For a sdof system under dual frequency excitations, the governing equation is:

$$\frac{\mathrm{d}^2u}{\mathrm{d}t^2} + f(u,\dot{u}) = (1-\varepsilon)p_1 \sin(\Omega_1 t) + \varepsilon p_2 \sin(\Omega_2 t). \tag{13}$$

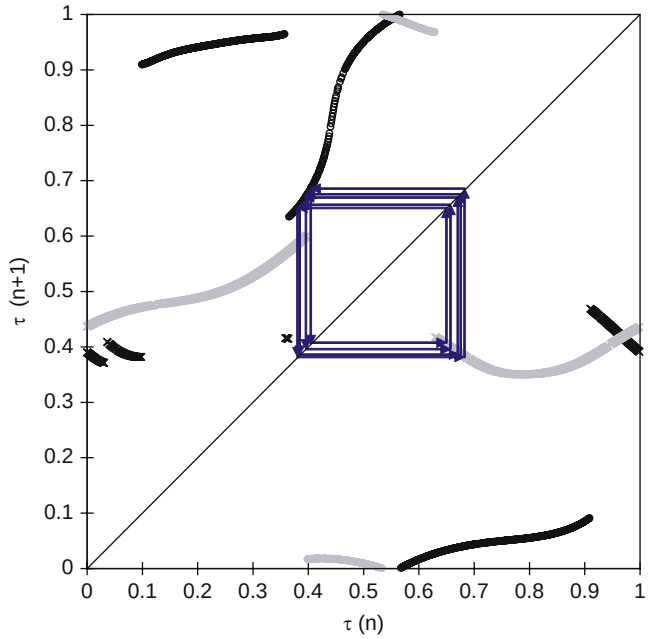

Fig. 9. Iterated maps of τ_1 and τ_3 for dual-frequency excitation ($\Omega_1 = 0.45, \Omega_2 = 0.9, \varepsilon = 0.2$), ×**p–p** map, ○ **p–m** map, × (gray) **m–p** map, ○ (gray) **m–m** map.

The parameter ε is introduced to control the relative amplitude between two applied excitations. The cases of $\varepsilon = 0$ and 1 correspond to uni-frequency oscillations. In order to study the frequency ratio dependence of commensurable frequency excitations, three sets of dual frequencies are selected: $\Omega_1 = 0.45$, $\Omega_2 = 0.9$; $\Omega_1 = 0.3$, $\Omega_2 = 0.9$; $\Omega_1 = 0.6$, $\Omega_2 = 0.9$. These frequencies make 1:2, 1:3, and 2:3 frequency ratios, respectively. From numerical simulations in the previous section, the 1:2 ratio excitation produces the most severe dynamic ratchetting. On the other hand, the 1:3 ratio does not produce dynamic ratchetting.

Fig. 9 shows the iterated maps, when $\Omega_1 = 0.45$, $\Omega_2 = 0.9$, and $\varepsilon = 0.2$. Motions evolve and eventually converge into a stable cycling that can be identified by two stable points, τ_1^* on the **m–p** map and τ_3^* on the **p–m** map. The absolute values of slopes of map functions at two stable points are slightly less than 1. Therefore, there is no bifurcation of the stable points. However, it takes a very long time for the motion to reach a stable cycling. If symbol **e** represents the elastic state, the stable cycling can be expressed as **e:p:e:m**, where : indicates the change of state. The two examples in Fig. 10 show the iterated maps when the frequency ratio is 1:3 ($\Omega_1 = 0.3, \Omega_2 = 0.9$). The stable cycling for $\varepsilon = 0.2$ is **e:p:e:m**, whereas it is **e:p:e:p:e:m:e:m** for $\varepsilon = 0.5$. In Fig. 10(b), two stable points (0.238 and 0.738) are on the **p–p** map and the **m–m** map. Fig. 11 shows iterated maps and stable cycling for $\varepsilon = 0.2$ and 0.5 when the frequency ratio is 2:3. The stable cycling for $\varepsilon = 0.2$ is **e:p:e:m:e:p:e:m**, and it becomes **e:p:e:m:e:p:e:p:e:m** for $\varepsilon = 0.5$. In Fig. 12, the stable points of stable cycling are depicted with varying ε values. The figures show that a unique stable cycling is developed for every ε.

It should be noted that the **p–p** map and the **m–m** map are needed for identifying stable cycling that includes **e:p:e:p** or **e:m:e:m** patterns. Under an uni-frequency excitation, a stable cycling contains neither the **p–p** map nor the **m–m** map, and the **m–p** map and the **p–m** map are the same shape. So either **p–m** or **m–p** map is sufficient to represent the motion as was utilized in [17].

5. Symmetry in dynamic ratchetting

In the previous section, it is shown that there exists a unique stable cycling for commensurable dual-frequency excitations. In the plastic regime of a stable cycling, it is interesting to notice that the plastic deformation is not an independent variable. So the existence of a stable cycling does not imply the boundedness of plastic deformation. Actually, dynamic ratchetting is related to the characteristics of

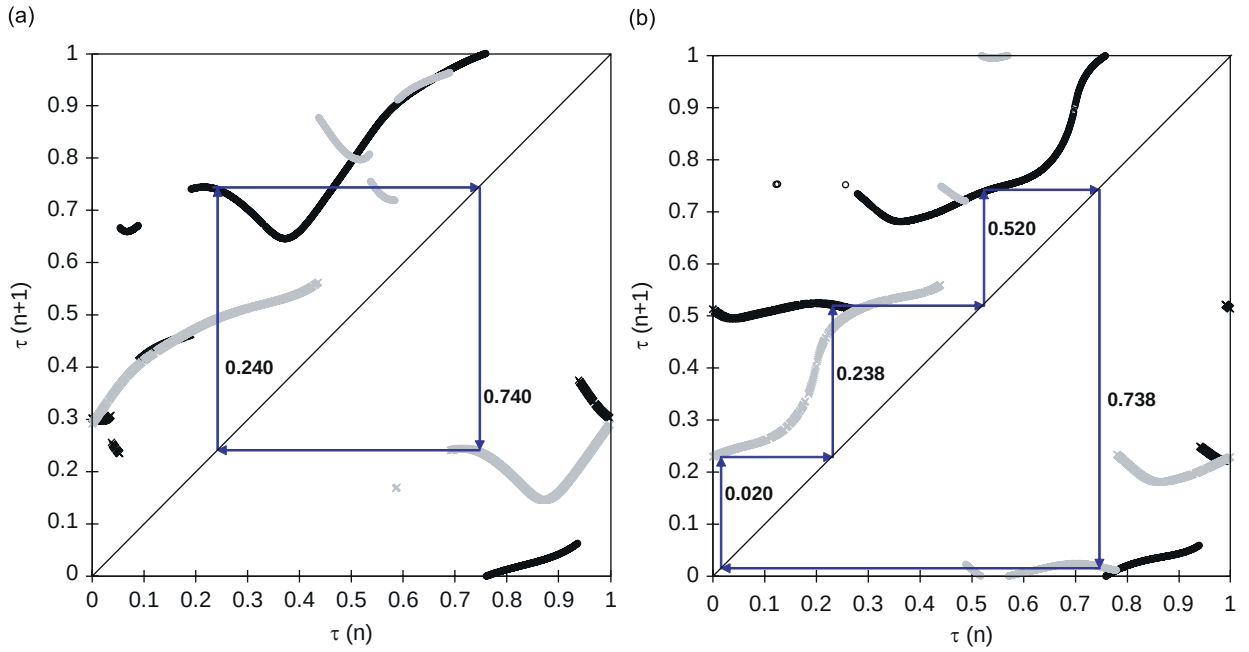

Fig. 10. Iterated maps of τ_1 and τ_3 for dual-frequency excitation ($\Omega_1 = 0.3, \Omega_2 = 0.9$): (a) $\varepsilon = 0.2$, (b) $\varepsilon = 0.5$, × **p–p** map, ○ **p–m** map, × (gray) **m–p** map, ○ (gray) **m–m** map.

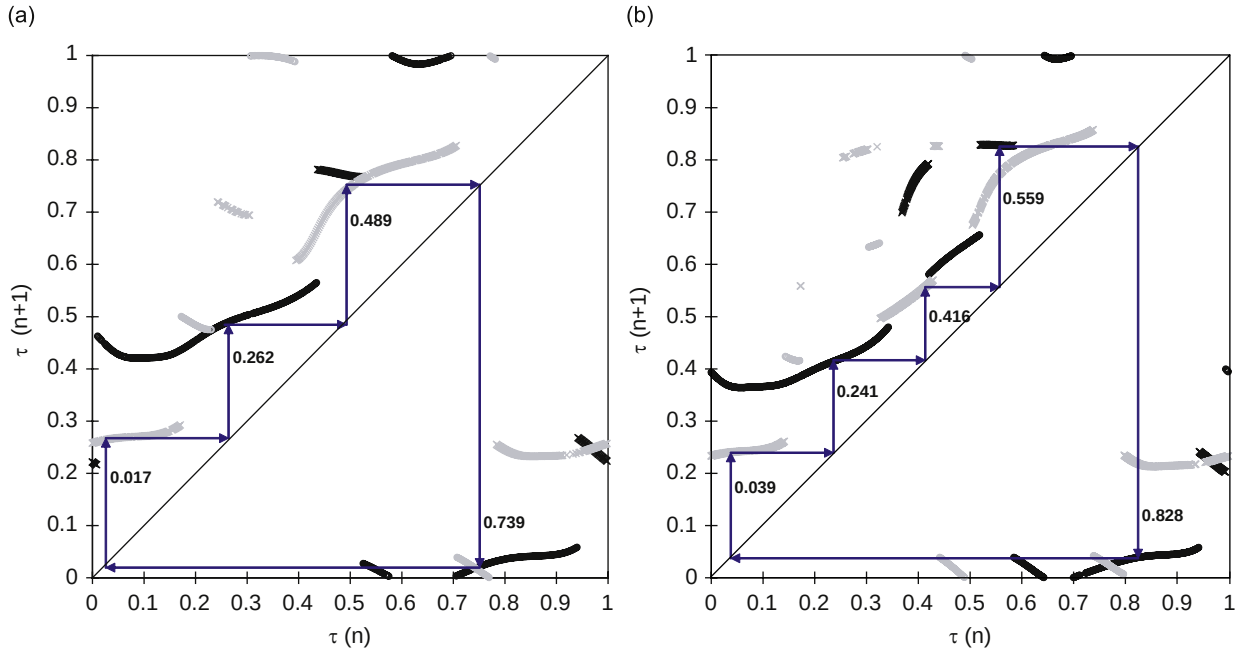

Fig. 11. Iterated maps of τ_1 and τ_3 for dual-frequency excitation ($\Omega_1 = 0.6, \Omega_2 = 0.9$): (a) $\varepsilon = 0.2$, (b) $\varepsilon = 0.5$, × **p–p** map, ○ **p–m** map, × (gray) **m–p** map, ○ (gray) **m–m** map.

excitations, which can be represented by the symmetry of iterated maps. Under commensurable frequencies, first, the symmetry of the **m–p** map and the **p–m** map needs to be discussed. When plastic deformations are separated into positive components and negative components, they can be canceled out if two iterated maps,

f_p^m (**m–p** map) and f_m^p (**p–m** map), have symmetry such that

$$f_p^m(\tau_1) = f_m^p(\tau_1 + 0.5) + 0.5,$$
$$f_m^p(\tau_3) = f_p^m(\tau_3 + 0.5) + 0.5. \tag{14}$$

This symmetry has been observed in iterated maps under uni-frequency excitations. Fig. 13 shows iterated maps of an uni-frequency excitation. Symmetry in Eq. (14) is shown as having the same shape between the sub-plane I and IV and between the sub-plane II and III in the figure with changes between the **p–p** map and the **m–m** map; and between the **m–p** map and the **p–m** map. The symmetric iterated maps also occur under 1:3 frequency ratio excitation (Fig. 10).

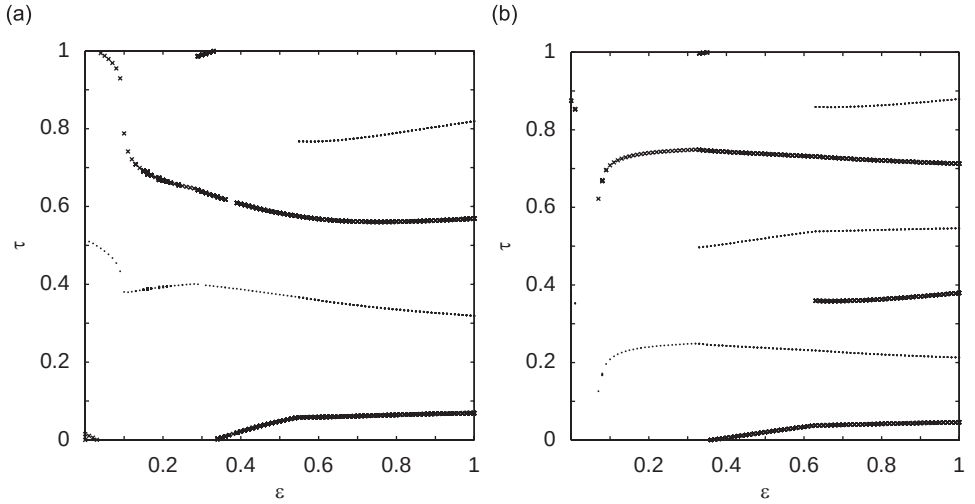

Fig. 12. Stable points of stable cycling in dual frequency excitations: (a) $\Omega_1 = 0.45$ $\Omega_2 = 0.9$, (b) $\Omega_1 = 0.3$ $\Omega_2 = 0.9$, • τ_1^*, × τ_3^*.

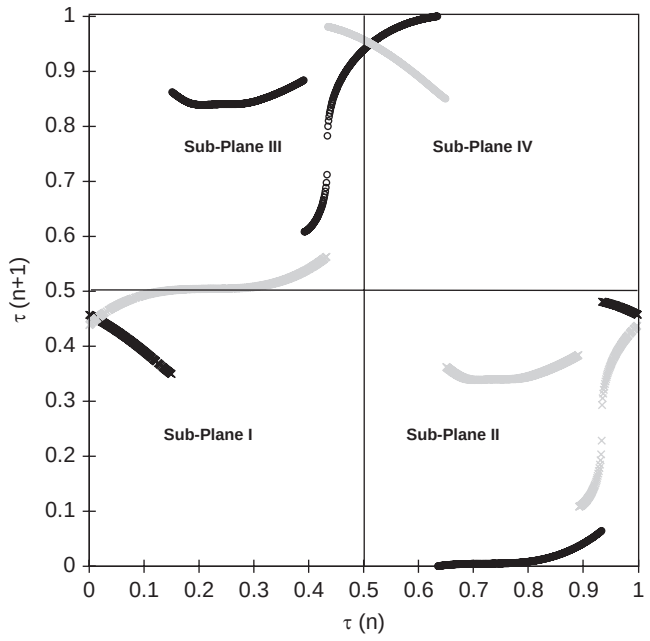

Fig. 13. Symmetry in iterated maps ($\Omega = 0.3, p = 1.0$): × **p–p** map, ○ **p–m** map, × (gray) **m–p** map, ○ (gray) **m–m** map.

When frequencies have commensurable ratios and their product makes an even number, the symmetry of iterated maps is broken and dynamic ratchetting is developed. The existence of this kind of symmetry is discussed further in the recent work by Challamel, Lanos, Hammouda, and Redjel [23]. The symmetry of iterated maps corresponds to a shift symmetry of an antiperiodic excitation function, $E(t) = -E(t + T/2)$, where T represents the period of the lower frequency excitation contained in $E(t)$. When this symmetry is broken, then the subject system can develop dynamic ratchetting, and this corresponds to the general symmetry requirements of ratchets [7,24].

Because dynamic ratchetting is directly related with excitation functions, these functions need to be selected with great care in analyses. For example, earthquake strong motions may contain commensurable frequency content that develop dynamic ratchetting. However, the selection of strong motion in design and assessment of structures has not been considered from this point of view yet, and results from analyzes may contain inconsistent dynamic ratchetting effects.

6. Summary and conclusions

In the present study, the characteristics of dynamic ratchetting are investigated based on numerical simulations, and iterated maps are derived from piecewise linear solutions. Piecewise linear solutions are derived for a sdof dynamic system having elasto-perfectly-plastic hysteretic damping under multi-frequency sinusoidal excitations. Iterated maps developed from piecewise solutions show that dynamic ratchetting occurs through a stable cycling.

Under commensurable frequency excitations, there is no dynamic ratchetting when the product of terms comprising the integer ratio is an odd number. For iterated maps, this condition exhibits symmetry between maps, which corresponds to general shift symmetry condition of antiperiodic excitation functions, $E(t) = -E(t + T/2)$, of ratchets. When the product of terms is an even number, the symmetry is broken and dynamic ratchetting occurs. The fact that the source of dynamic ratchetting exists in the excitation functions emphasizes the importance of excitation function selection in nonlinear dynamic analysis, such as in earthquake engineering and seismic design.

Even though it is not discussed in the present paper, numerical simulations of various sdof and mdof (Multi Degrees of Freedom) systems under recorded earthquake strong motions do indicate dynamic ratchetting. Application of an iterated maps approach to these systems, however, is not straight forward because of the increased number of variables.

References

[1] G.A. Maugin, *The Thermomechanics of Plasticity and Fracture*, Cambridge University Press, Cambridge, England, New York, 1992.
[2] A.K. Chopra, *Dynamics of Structures: Theory and Applications to Earthquake Engineering*, Prentice-Hall, Upper Saddle River, NJ, 2001.
[3] T.T. Soong, G.F. Dargush, *Passive Energy Dissipation Systems in Structural Engineering*, Wiley, Chichester, England, 1997.
[4] I.-S. Ahn, S.S. Chen, G.F. Dargush, Dynamic ratcheting in elastoplastic single-degree-of-freedom systems, *Journal of Engineering Mechanics—ASCE* 132 (2006) 411–421.
[5] I.-S. Ahn, Dynamic Ratchetting in Hysteretic Damping Systems, PhD Dissertation, Department of Civil, Structural and Environmental Engineering, University at Buffalo, Buffalo, NY, 2005.
[6] S. Denisov, L. Morales-Molina, S. Flach, P. Hänggi, Periodically driven quantum ratchets: symmetries and resonances, *Physical Review A* 75 (2007) 063424.
[7] P. Reimann, Brownian motors: noisy transport far from equilibrium, *Physics Reports* 361 (2002) 57–265.
[8] T. Hassan, S. Kyriakides, Ratchetting in cyclic plasticity: part I, uniaxial behavior, *International Journal of Plasticity* 8 (1992) 91–116.
[9] S.W. Shaw, P.J. Holmes, Periodically forced linear oscillator with impacts: chaos and long-period motions, *Physical Review Letters* 51 (1983) 623–626.
[10] S.W. Shaw, P.J. Holmes, A periodically forced impact oscillator with large dissipation, *Journal of Applied Mechanics—ASME* 50 (1983) 849–857.
[11] S.W. Shaw, P.J. Holmes, A periodically forced piecewise linear oscillator, *Journal of Sound and Vibration* 90 (1983) 129–155.
[12] S. Natsiavas, On the dynamics of oscillators with bi-linear damping and stiffness, *International Journal of Non-Linear Mechanics* 25 (1990) 535–554.
[13] S. Natsiavas, Stability of piecewise linear oscillators with viscous and dry friction damping, *Journal of Sound and Vibration* 217 (1998) 507–522.

[14] E. Pavlovskaia, M. Wiercigroch, C. Grebogi, Modeling of an impact system with a drift, *Physical Review E* 64 (2001) 056224.
[15] E. Pavlovskaia, M. Wiercigroch, Modeling of vibro-impact system driven by beat frequency, *International Journal of Mechanical Sciences* 45 (2003) 623–641.
[16] E. Pavlovskaia, M. Wiercigroch, Analytical drift reconstruction for visco-elastic impact oscillators operating in periodic and chaotic regimes, *Chaos, Solitons & Fractals* 19 (2004) 151–161.
[17] G.R. Miller, M.E. Butler, Periodic response of elastic-perfectly plastic sdof oscillator, *Journal of Engineering Mechanics—ASCE* 114 (1988) 536–550.
[18] H. Poincaré, *New Methods of Celestial Mechanics (Trans. of Les Méthodes Nouvelles de la Mécanique Céleste)*, Guthier-Villars, Paris, 1892.
[19] V.I. Arnold, *Ordinary Differential Equations*, MIT Press, Cambridge, Massachusetts, London, England, 1973.
[20] J. Guckenheimer, P. Holmes, Nonlinear oscillations, dynamical systems, and bifurcations of vector fields, *Applied Mathematical Sciences*, vol. 42, Springer, New York, 1983.
[21] R.L. Devaney, *An Introduction to Chaotic Dynamical Systems*, Addison-Wesley, Redwood City, California, 1989.
[22] R.C. Hilborn, *Chaos and Nonlinear Dynamics*, Oxford University Press, New York, 2000.
[23] N. Challamel, C. Lanos, A. Hammouda, B. Redjel, Stability analysis of dynamic ratcheting in elastoplastic systems, *Physical Review E* 75 (2007) 026204.
[24] S. Flach, O. Yevtushenko, Y. Zolotaryuk, Directed current due to broken time-space symmetry, *Physical Review Letters* 84 (2000) 2358–2361.